Selective skeletal editing of polycyclic arenes using organophotoredox dearomative functionalization

Wei Wang (wwang@pharmacy.arizona.edu)
University of Arizona https://orcid.org/0000-0001-6043-0860

Peng Ji
University of Arizona

Cassondra Davies
Oberlin College

Feng Gao
University of Arizona

Jing Chen
University of Arizona

Xiang Meng
University of Arizona

Kendall Houk
University of California Los Angeles https://orcid.org/0000-0002-8387-5261

Shuming Chen
Oberlin College https://orcid.org/0000-0003-1897-2249

Article

Keywords:

Posted Date: January 5th, 2022

DOI: https://doi.org/10.21203/rs.3.rs-1139594/v1

Version of Record: A version of this preprint was published at Nature Communications on August 5th, 2022. See the published version at https://doi.org/10.1038/s41467-022-32201-7.

Selective skeletal editing of polycyclic arenes using organophotoredox dearomative functionalization

Peng Ji,[1] Cassondra C. Davies,[2] Feng Gao,[1] Jing Chen,[1] Xiang Meng,[1] K. N. Houk,[3]* Shuming Chen[2]* and Wei Wang[1]*

[1]Departments of Pharmacology and Toxicology and Chemistry and Biochemistry, University of Arizona, Tucson, AZ 85721-0207, USA

[2]Department of Chemistry and Biochemistry, Oberlin College, Oberlin, OH 44074, USA

[3]Department of Chemistry and Biochemistry, University of California, Los Angeles, CA 90095-1569, USA

Abstract

Reactions that lead to destruction of aromatic ring systems often require harsh conditions and, thus, take place with poor selectivities. Selective partial dearomatization of fused arenes is even more challenging but it can be a strategic approach to creating versatile, complex polycyclic frameworks. Herein we describe a general organophotoredox approach for the chemo- and regioselective dearomatization of structurally diverse polycyclic aromatics, including quinolines, isoquinolines, quinoxalines, naphthalenes, anthracenes and phenanthrenes. The success of the new method for chemoselective oxidative rupture of aromatic moieties relies on precise manipulation of the electronic nature of the fused polycyclic arenes. Experimental and computational results show that the key to overcoming the intrinsic thermodynamic and kinetic unfavorability of the dearomatization process is an ultimate hydrogen atom transfer (HAT) step, which enables dearomatization to predominate over the otherwise favorable aromatization pathway. We show that this strategy can be applied to rapid synthesis of biologically valued targets and late-stage skeletal remodeling *en route* to complex structures.

Polycyclic scaffolds bearing partially dearomatized fused arenes are commonly encountered in natural products, pharmaceuticals and bioactive molecules[1-5]. While these molecular frameworks lead to great structural diversity and intriguing biological properties, they engender synthetic challenges as their assembly often requires prefunctionalized substrates and multi-step sequences. Direct dearomatization of fused arenes constitutes an outstandingly efficient approach for the construction of polycyclic scaffolds due to its high atom and step economy[1-5]. However, selective dearomatization and functionalization of fused arenes is difficult because harsh conditions are often required to disrupt aromaticity, leading to poor selectivities. As a result, dearomative functionalizations of fused arenes has been largely limited to activated arenes such as indoles[6-15] and naphthols[16-20].

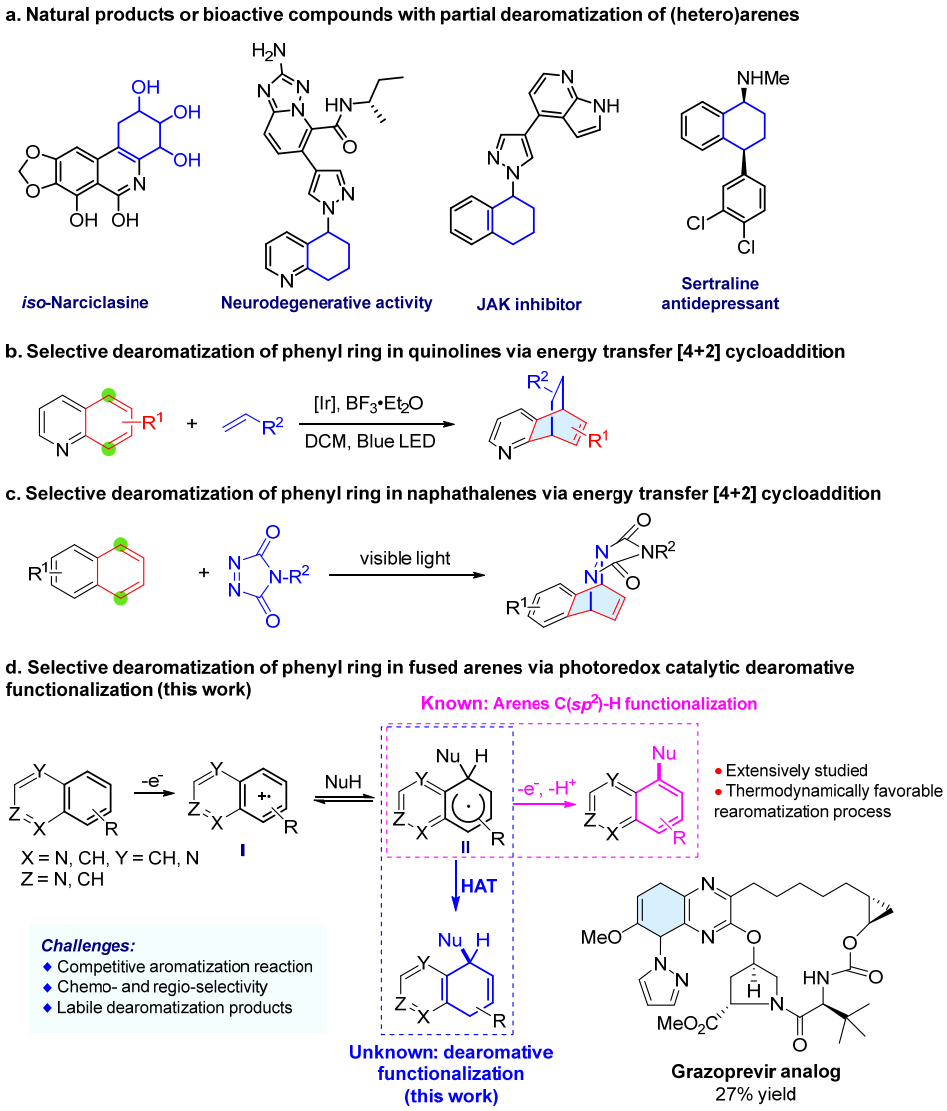

Figure 1. Methods for selective dearomative functionalization of fused arenes. a, Examples of partially dearomatic natural products and bioactive compounds. **b,** Selective dearomatization of quinolines. **c**, Selective dearomatization of naphthalenes. **d**, Selective dearomatization of structurally diverse fused arenes (this work).

Issues of chemo- and regioselectivity also add to the difficulty of dearomative functionalizations of unactivated fused arenes such as quinolines and naphthalenes. Selective dearomatization of pyridine moieties in fused arenes is feasible[21-25] owing to the electron deficient nature of pyridine and assistance provided by Lewis acid complexation. Selective dearomatization of phenyl moieties in fused arenes, on the other hand, is significantly more challenging. To our knowledge, only one example has been described in a recent report by Brown, Houk and Glorius involving a photochemical [4+2] cycloaddition between quinolines and alkenes (Figure 1b)[26] enabled by energy transfer and Lewis acid activation. A similar [4+2] cycloaddition strategy initiated by energy transfer was also employed in the dearomatization of naphthalene by Sarlah *et al*. (Figure 1c)[27-32].

We wondered if a photoredox strategy could be used to selectively dearomatize the phenyl moieties in quinolines, isoquinolines, quinoxalines, naphthalenes and other fused arenes. In reported photoredox processes, radicals add selectively to the pyridine ring in quinolines[33,34], and indiscriminately to the phenyl rings in naphthalenes. In contrast to Sarlah's [4+2] cycloaddition strategy, in which regioselectivity is governed primarily by steric effects[27,32], we envisaged taking advantage of the relative electron richness of the phenyl ring to achieve selective dearomative functionalization (Figure 1d). Photocatalytically promoted single electron transfer (SET) oxidation of quinolines would produce radical cation **I**, in which the positive charge is mostly localized on the phenyl ring. We anticipated nucleophiles to add to intermediate **I** selectively to form radical **II**. Direct arene C(sp^2)-H functionalization with nucleophiles under photoredox catalysis or electrophotochemical conditions have been elegantly leveraged by Nicewicz[35-38], Lambert[39], Hu[40], and Wickens[41] to generate aromatic functionalized products. We postulated that it would be possible to direct the reaction toward the less thermodynamically stable dearomatized products by capturing radical **II** with a sufficiently activated hydrogen atom transfer (HAT) agent. Below, we describe the successful development of a general chemo- and regioselective method for the dearomative functionalization of diverse fused arenes using this strategy.

Dearomatization of quinolines, isoquinolines, and quinoxalines

In order to undergo selective photoredox promoted dearomative functionalization, fused arenes must have oxidation potentials that enable them to be oxidized by excited states of photocatalysts (PCs) through SET. The oxidation potential of unsubstituted quinoline (E^{ox} = 2.23 V vs SCE, Supplementary Figure S1 and S2) suggests that its oxidation would be very difficult using common PCs. However, introduction of an OMe group onto the phenyl moiety of quinoline lowers the oxidation potential sufficiently (e.g., 6-methoxyquinoline **1a**, E^{ox} = 1.83 V vs SCE, Table 1 and Supplementary Figure S2), making it possible for it to participate in thermodynamically driven SETs with excited states of conventional organophotoredox catalysts such as acridinium and triphenylpyrylium (TPT) salts that have excited state reduction potentials (E^{*red}) greater than 2.0 V (Table 1).

Table 1. Exploration and optimization of reaction conditions.

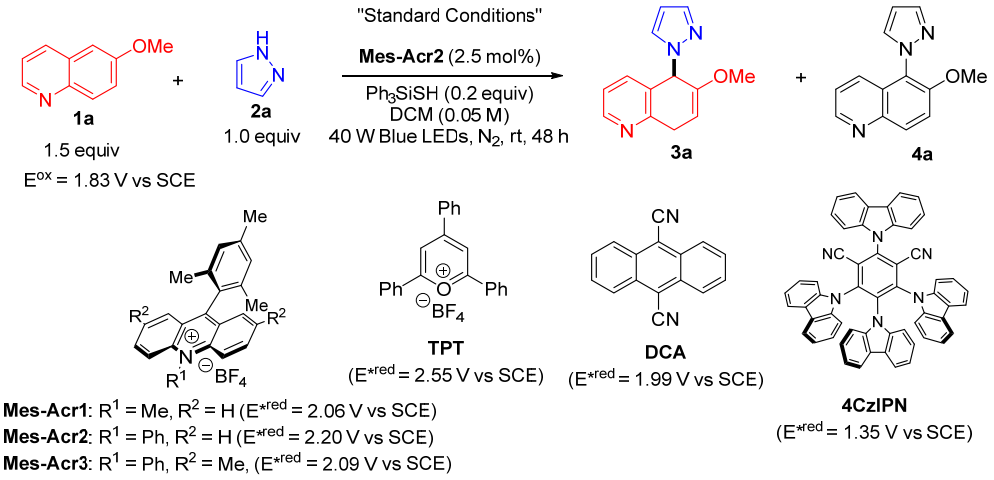

Entry	Variation from the "Standard Conditions"[a]	Yield[b] (%)
1	None	81, 76[c] (<5 of **4a**)[b]
2	**Mes-Acr1** instead of **Mes-Acr2**	75
3	**Mes-Acr3** instead of **Mes-Acr2**	67
4	**DCA** instead of **Mes-Acr2**	34
5	**TPT** instead of **Mes-Acr2**	18
6	**4CzIPN** instead of **Mes-Acr2**	trace
7	DCM (0.5 M) with 2,6-lutidine (0.2 equiv)	20
8	DCM (0.2 M) with 2,6-lutidine (0.2 equiv)	49

9	DCM (0.1 M) with 2,6-lutidine (0.2 equiv)	63
10	DCM (0.05 M) with 2,6-lutidine (0.2 equiv)	76
11	DCM (0.025 M) with 2,6-lutidine (0.2 equiv)	74
12	without Ph_3SiSH	53 (23 of **4a**)[b]
13	without **Mes-Acr2**	trace
14	without light	trace
15	390 nm light	40
16	O_2 instead of N_2	trace (56 of **4a**)[b]

[a]Standard conditions: unless otherwise specified, a mixture of 6-methoxyquinoline **1a** (0.3 mmol, 0.05 M), pyrazole **1b** (0.2 mmol), Ph_3SiSH (0.04 mmol), and **Mes-Acr2** (0.005 mmol) in DCM (under a N_2 atmosphere at room temperature was irradiated with 40 W Kessil blue LEDs for 48 h. [b]Yield determined by using ^{1}H NMR spectroscopy using 1,3,5-trimethoxybenzene as an internal standard. [c]Isolated yield.

We assessed the viability of the proposed dearomative functionalization protocol by reacting 6-methoxyquinoline **1a** with pyrazole **2a** as a nucleophile under irradiation with blue LEDs in DCM solutions containing HAT agents and commercially available organic photosensitizers (Table 1). The desired dearomatization product **3a** is generated in the highest yield using 1.5 equiv of **1a**, 1.0 equiv of **2a** (0.05 M), 2.5 mol% *N*-methylmeso-acridinium tetrafluoroborate (**Mes-Acr1**), 0.2 equiv of the HAT agent and 0.2 equiv of 2,6-lutidine. Nucleophile addition occurred exclusively at the 5-position. The efficiency of the reaction is dependent on the HAT agent (Supplementary Table S1). Among the 17 different thiols and benzeneselenols screened, Ph_3SiSH was found to be the superior HAT agent, leading to regioselective formation of **3a** in 81% yield (Table 1, entry 1). While photocatalysts such as **TPT** (E^{*red} = 2.55 V vs SCE, 18%, entry 4) with excited state reduction potentials higher than the oxidation potential of **1a** were found to promote this reaction, **Mes-Acr2** (2.5 mol%, = 2.2 V vs SCE) was identified as the best photocatalyst (**3a** formed 81% ^{1}H NMR yield, entry 1). Solvent has a significant effect on the reaction (Supplementary Table S2). Furthermore, substrate ratio (Supplementary Table S3) and concentration has a marked impact on the yield (entries 7-11) with low concentrations of **1a** being more beneficial (entries 7 vs 10). The absence of 2,6-lutidine does not affect the reaction outcome (entries 1 vs 10) as quinoline **1a** can serve as the base. Lastly, control experiments confirmed that the HAT agent, light and photocatalyst are all required for selective dearomatization. In particular, the HAT agent is critical for minimizing the formation of the aromatization product **4a** (entries 1 vs 12).

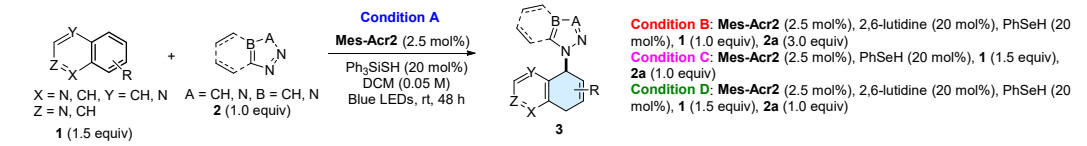

a. Scope of quinolines, isoquinoline, quinoxalines and azoles

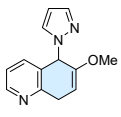

A: 3a, 76%

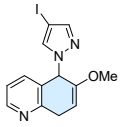

A: **3b**, 69%

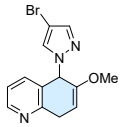

A: 3c, 61%

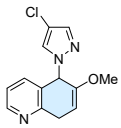

A: 3d, 53%

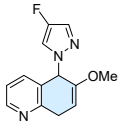

B[e]: 3e, 33%

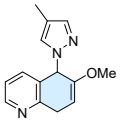

A: **3f,** 53%

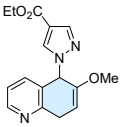

A: 3g, 67%

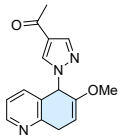

C: 3h, 63%

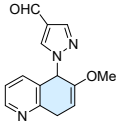

C: 3i, 34%

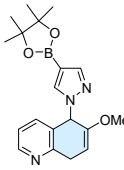

A: 3j, 51%

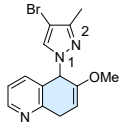

A: **3k**, 51% (N_1:N_2 = 7:1)[b]

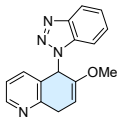

C: 3l, 25%

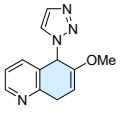

B[e]: 3m, 39%

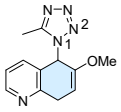

B[e]: 3n, 54% (N_1:N_2 =1.3:1)[b]

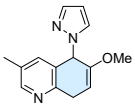

A: **3o**, 72%

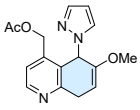

A: 3p 62%

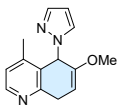

A: 3q, 65%

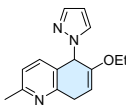

A: 3r, 51%

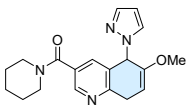

C: 3s, 22% (76% s.m.)

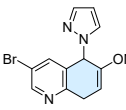

C: **3t,** 43%

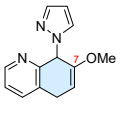

C: 3u, 45%

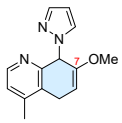

B: 3v, 43%

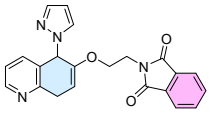

A: 3w, 41%

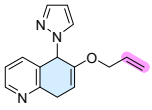

A: 3x, 59%

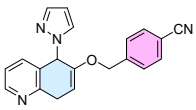

A: 3y, 83%

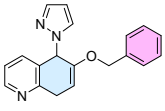

A: **3z**, 67%

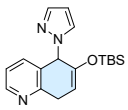

A: 3aa, 79%

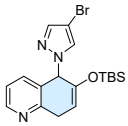

A: 3ab, 51%

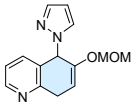

A: **3ac**, 81%

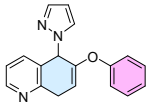

A: 3ad, 42%

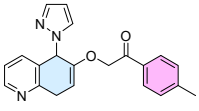

A: 3ae, 74%

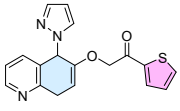

A: 3af, 86%

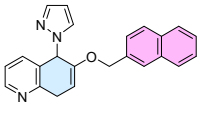

A: **3ag,** 37%

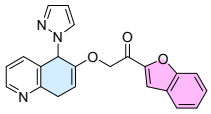

A: 3ah, 85%

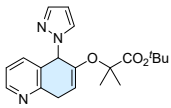

A: 3ai, 63%

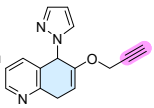

A: 3aj, 31% (s.m. 65%)[c]

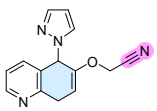

A: 3ak, 32% (s.m. 70%)[c]

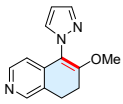

B: 3al, 43%

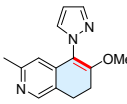

B: 3am, 39%

A: **3an,** 40%

b. Late stage modification

Viqualine

A: 3ao, 79%, dr^b = 1.1 : 1

C: 3ap, 43% (5 d), dr^d = 1.3 : 1

Galactose

A: 3aq, 32%

Galactose

C: 3ar, 35%, dr^d = 1.2:1

Menthol derivative

A: 3as, 56%, dr^d = 1.1 : 1

Probalan derivative

A: 3at, 39%

Tyrosine derivative

C: 3au, 43%

Cholesterol derivative

C: 3av, 31% (+ 45% s.m.), dr^d = 1 : 1

Estrone derivative

A: 3aw, 47%, dr^d = 1.5 : 1

Grazoprevir analog

A[f]: 3ax, 27%, dr^d = 1 : 1

Figure 2. Scope of photoredox dearomative functionalization of quinolines, isoquinolines, and quinoxalines with azoles. **a,** Scope of quinolines and quinoxalines with azoles. **b,** Late-stage functionalization. [a]Reaction conditions: unless otherwise specified, see footnote a of Table 1 and supplementary materials; [b]Ratio of isomers was determined by using ^{1}H NMR analysis of the crude reaction mixture; [c]s.m.: starting materials; [d]dr value was determined by ^{1}H NMR analysis of the crude reaction mixture; [e]Condition B without 2,6-lutidine; [f]Condition A using 3,6-di-*tert*-butyl-9-mesityl-10-phenylacridin-10-ium tetrafluoroborate as photocatalyst for 5 d.

Having established optimal conditions for the new photoredox promoted dearomative functionalization reaction, we next explored the scope with fused arenes as substrates and azoles as nucleophiles (Figure 2a). Our results show that the reaction proceeds with high chemo- and regioselectivity for a wide range of quinolines and azoles. Both electron-donating and electron-withdrawing groups are tolerated on the pyrazole. Halogenated pyrazoles reacted with 6-methoxyquinoline with Ph_3SiSH as the HAT agent (condition A giving **3b**-**3d**). For 5-fluoropyrazole, benzeneselenol, which is 10-fold more reactive than thiols in HAT[42,43], is required along with 2,6-lutidine (condition B) to yield **3e**. Other electron-deficient pyrazoles also reacted in the presence of benzeneselenol to produce **3h** and **3i** (condition C, without 2,6-lutidine). Notably, the dearomatization method can be applied to a pyrazole boronate, which generates **3j** (51%) containing a useful handle for subsequent coupling reactions. A disubstituted pyrazole also reacted smoothly to form **3k** (51%), as did other common azoles including benzotriazole (**3l**), 1,2,3-triazoles (**3m**), and tetrazole (**3n**) under condition B or C.

6-Alkoxy-substituted quinolines are particularly effective substrates for the dearomative functionalization reaction, producing diverse substituted 5,8-dihydroquinolines as products (Figure 2a). A wide range of alkoxy substituents, including those containing methyl (**3o**, **3q**, **3r**, and **3v**), ester (**3p, 3ai**), bromo (**3t**), amide (**3s**), phthalimide (**3w**), alkene (**3x**), benzyl (**3y**, **3z**), TBS (**3aa, 3ab**), MOM (**3ac**), phenyl (**3ad**), ketone (**3ae**), alkyne (**3aj**), nitrile (**3y**, **3ak**), thiophene (**3af**) and benzofuran (**3ag**) moieties, are well tolerated. Moreover, the process promotes selective dearomatization and functionalization of quinoline ring systems even when other arene moieties including benzene (**3w**, **3y**, **3z**, **3ad**, **3ae**), thiophene (**3af**) and benzofuran (**3ah**) are present. Notably, the protocol enables highly selective dearomatization of a quinoline (E^{ox} = 1.86 V vs SCE) over a naphathalene (E^{ox} = 1.92 V vs SCE) ring (**3ag**) despite their similar oxidation potentials. In addition to controlling chemoselectivity, 6-alkyloxy groups also direct site selective formation of

5-nucleophile-substituted-5,8-dihydroquinolines. Furthermore, dearomatization of 7-methoxyquinolines is also highly regioselective generating only 8-substituted 5,8-dihydroquinoline products (**3u**, **3v**). Isoquinolines can participate in the process (**3al, 3am**). However, regioisomeric 7,8-dihydroisoquinolines are formed. Finally, quinoxalines are also viable substrate for the dearomatization process (**3an**).

Owing to the mild conditions required, the organophotoredox-promoted dearomative functionalization process is applicable to late-stage functionalizations of complex pharmaceutically relevant quinoline structures including viqualine (**3ao**), Oppolzer's camphorsultam (**3ap**), galactose (**3aq**, **3ar**), menthol (**3as**), probalan (**3at**), tyrosine (**3au**), cholesterol (**3av**), and estrone (**3aw**) groups (Figure 2b). It is particularly impressive that a grazoprevir analog (**3ax**) containing various functional groups was selectively dearomatized utilizing this process. These results underscore the mildness, high chemo- and regioselectivity, and practicality of the new protocol.

Dearomatization of fused arenes

Encouraged by the success of the new photoredox reaction of quinolines, we explored its utility for the selective dearomatization of fused non-heteroaromatics. The results show that selective dearomatization of fused arenes is more challenging. As with quinolines, electron-donating substituents can be used to lower the oxidation potentials and enhance reactivity. A 2-methoxy substituent in naphthalene, for instance, lowers the oxidation potential to 1.8 V (vs SCE, supplementary Figure S2) and enables selective oxidation by the excited state of photocatalyst **Mes-Acr2**. Selective dearomatization and C-1 functionalization of 2-methoxynaphthalene by pyrazole using condition B led to **3ay** (Figure 3a). The efficiency of this process is also dependent on the base and the HAT agent, as are shown in **3az**, **3ba**, and **3bi** (condition C), **3bb, 3bf, 3bg, 3bh,** and **3bj** (condition B) and **3be** (condition D). The dearomatization strategy can be applied to methyl substituted naphthalene (**3bd**). Finally, unsubstituted naphthalene (**3bd**) also participates in the process to produce the 1-substituted product regioselectively.

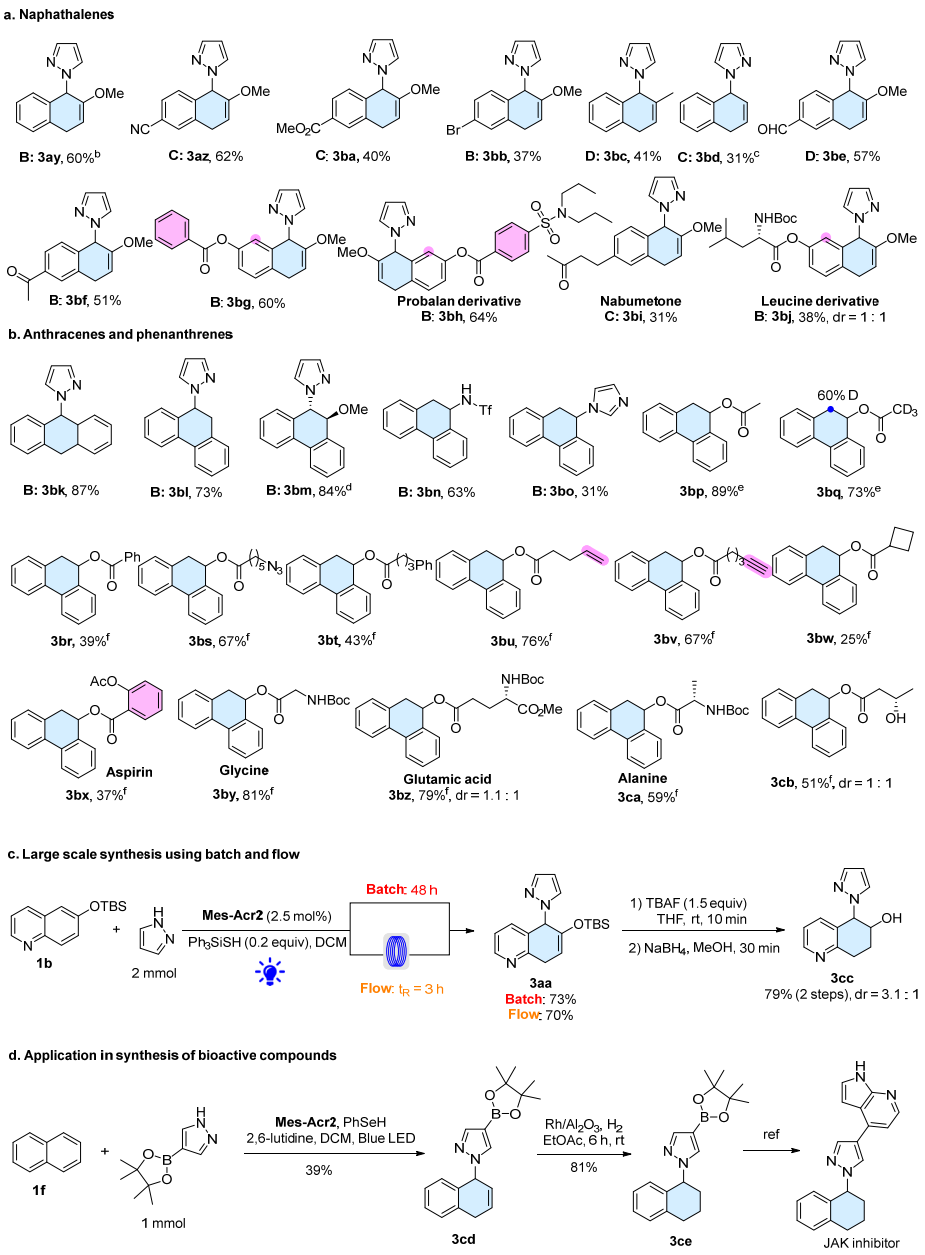

Figure 3. Dearomatization of fused arenes. **a,** Scope of naphathalenes. **b**, Scope of anthracenes and phenanathrenes. **c**, Large scale synthesis. **d,** Application in synthesis of valuable targets. [a]Reaction condition: unless specified, see footnote a of Table 1 and the ESI; [b]Ratio of 6-methoxynaphthalene to pyrazole: 1 : 2; [c]Ratio of naphthalene to pyrazole is 2:1; [d]Reaction time: 4 d; [e]Condition B using10.0 equiv of acid; [f]Condition B using 5.0 equiv of acid.

The photoredox reaction can also be applied to the dearomatization functionalization of other common polycyclic aromatic hydrocarbons including anthracene (**3bk**, 87%) and phenanthrene (**3bl**, 73%) (Figure 3b). Notably, 6-methoxyphenanthrene reacts to form the *trans* substitution

product **3bm** (84%). Moreover, nucleophiles other than azoles, such as trifluoromethanesulfonamide (**3bn**) and imidazole (**3bo**), can also participate in the process. Furthermore, carboxylic acids, which are often used as radical precursors in photoredox reactions[44], serve as effective nucleophiles for dearomative functionalization of phenanthrenes. These reactions proceed in moderate to high yields (**3bp**-**3cb**, 25-89%) and display broad functional group tolerance including phenyl (**3br**, **3bt**), azide (**3bs**), alkenyl (**3bu**), alkynyl (**3bv**), cyclobutyl (**3bw**), and hydroxyl acid groups (**3cb**). Due to their weaker nucleophilicity and steric effects, benzoic acid (**3bx**) and secondary carboxylic acids (**3bw**) are less effective nucleophiles for this process. In addition, the reaction can be utilized for the direct modification of biologically relevant structures such as aspirin (**3bx**) and amino acids (**3by-3ca**).

Studies with the silyloxyquinoline **1b** show that the synthetic protocol can be scaled up without loss of yield (Figure 3c). Moreover, the reaction can be adapted for use in a flow system, an emerging technology in organic synthesis[45]. Using the flow system, the reaction time is reduced dramatically to 3 h without compromising the yield. The product silylenol ether **3aa** can be converted to the corresponding alcohol **3cc**. The preparative power of the new method was also demonstrated by its use in the cost-effective synthesis of important biologically active targets, including a JAK inhibitor (Figure 3d)[46]. Our new synthetic route starts from naphthalene ($0.04/g) instead of the more expensive 1-bromo-1,2,3,4-tetrahydronaphthalene ($370/g) used in the earlier preparative pathway[46]. Dearomatization of naphthalene with pyrazol-4-ylboronic acid pinacol ester produces key intermediate **3cd**, which is then reduced using Rh/Al_2O_3 catalyzed hydrogenation to form **3ce**. The JAK inhibitor is then readily prepared from **3ce** using reported procedures[46]. These studies clearly demonstrate the synthetic value of the our dearomative functionalization protocol, which provides direct and efficient access to polycyclic partially dearomatized frameworks that were previously inaccessible or required strenuous synthetic efforts.

Mechanistic studies. To gain insight into the reaction mechanism, chemo- and regioselectivity and the role played by the HAT agent, we conducted computational studies and additional experiments. The excited state PC^{+}***** **Mes-Acr2*** possesses strong oxidizing power (E^{red}***** = 2.2 V) and can oxidize the 6-methoxyquinoline (**1a**) (E^{ox} = 1.83 V vs SCE, supplementary Figure S1) to give radical cation **5a** (Figure 4a and Stern-Volmer quenching experiments, supplementary Figure S3). The oxidation potential of the fused arene substrate is crucial for the success of this process,

as demonstrated by the high reactivity of **1a** in contrast to the lack of reactivity of unsubstituted quinoline (E^{ox} = 2.23 V vs SCE, Supplementary Figure S2). In addition, when a mixture of **1a** and 6-acetoxyquinoline (**1c**) (E^{ox} = 2.2 V vs SCE, supplementary Figure S2) is subjected to the reaction conditions, only **1a** undergoes selective dearomatization to form **3a**, indicating that electron-withdrawing substituents inhibit the reaction. In contrast, **1a** and 2-methoxynaphthalene (**1e**, E^{ox} = 1.8 V vs SCE, Supplementary Figure S2), which have similar oxidation potentials, both react under the same conditions to produce the corresponding dearomatized products **3a** and **3ay** (Figure 4b). Likewise, phenanthrene **1d** (E^{ox} = 1.91 V vs SCE, Supplementary Figure S2) is an effective substrate for this process (Figure 4b). Notably, the pyrazole nucleophile (E^{ox} = 2.15 V vs SCE, Supplementary Figure S2) is not oxidized by **Mes-Acr2***. This is supported by luminescence quenching study of **Mes-Acr2** with varying concentrations of 6-methoxyquinoline **1a** and pyrazole **2a** (Supplementary Figure S4).

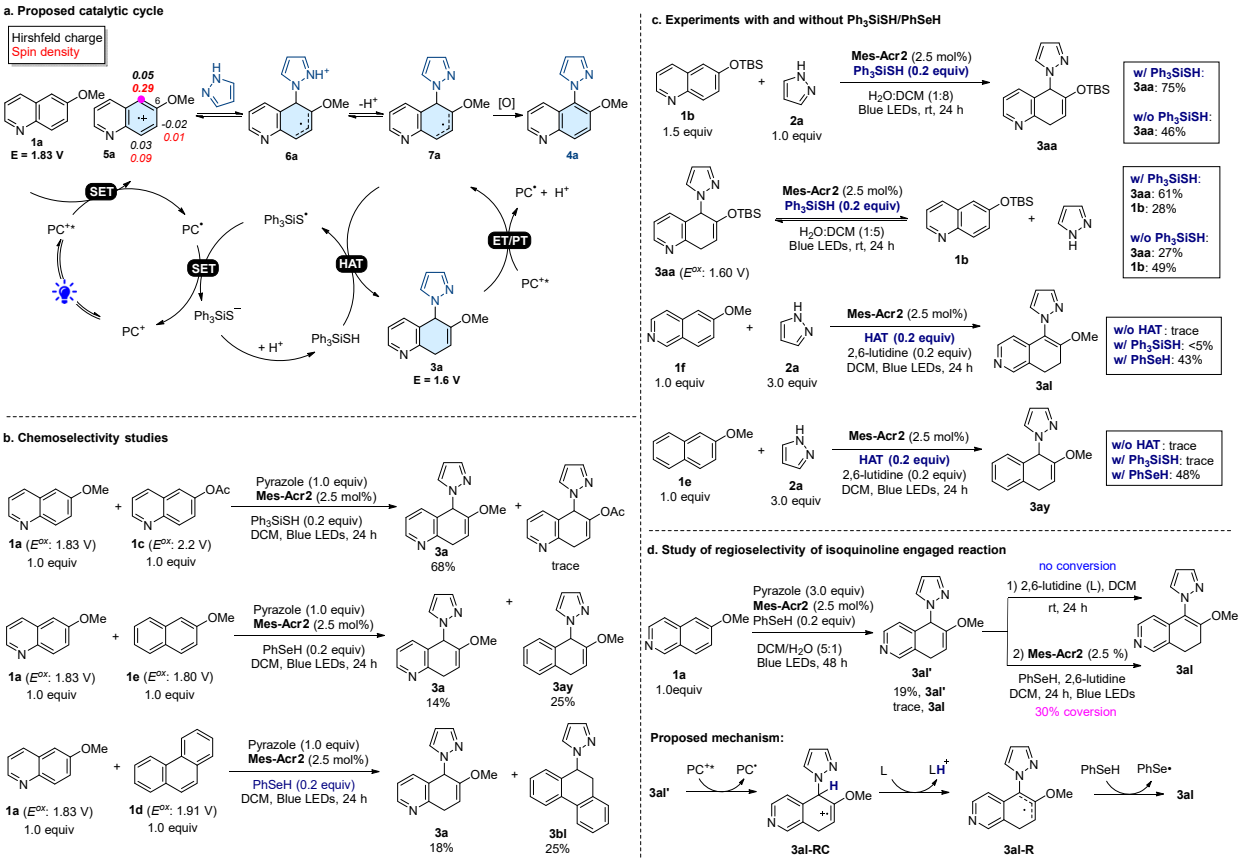

Figure 4. Mechanistic studies. **a,** Proposed catalytic cycle. **b,** Chemoselectivity studies. **c,** Study of roles of HAT reagent. **d,** Study of regioselectivity of isoquinoline engaged reaction.

Following the oxidation of **1a** through SET, pyrazole reacts with the electrophilic radical cation **5a** to form the radical cation **6a** (Figure 4a). Calculated Hirshfeld charge and spin densities (Figure 4a; see Supplementary Figure S5 for calculated charge and spin densities for other substrates) indicate that C5 has the highest spin density (bold face) in **5a** and is therefore the preferred site for nucleophilic addition. The calculated free energies also support the observation that reaction at C5 position is kinetically favored over C8 or C7 by at least 3 kcal/mol (Supplementary Figure S6). Subsequent exothermic deprotonation of **6a** by 2,6-lutidine gives the neutral radical **7a**. Calculated free energies suggest that sequential SET oxidation and deprotonation of **7a** to form the aromatic substitution product **4a** is more thermodynamically favorable (-24.9 kcal/mol, Figure 5). This is reflected in the outcomes of processes leading to fully aromatic products developed by Nicewicz[35-38], Lambert[39], Hu[40] and Wickens[41]. However, the presence of a reactive HAT agent (e.g., Ph_3SiSH) redirects the course of the reaction toward the dearomatized product **3a** rather than the more stable aromatic product **4a** (Figure 5). The transformation of **7a** into **3a** is facilitated by the exergonic nature of the HAT step (-17.4 kcal/mol change in free energy). Thus, success of the dearomatization process depends on the use of thiol and selenol HAT agents that have weak S-H and Se-H bonds (S-H: 82 kcal/mol, Se-H: 73 kcal/mol) and correspondingly high H-atom transfer rates (PhSH: $K_{20} = 9.0 \times 10^7$ $M^{-1}S^{-1}$ and PhSeH: $K_{20} = 1.3 \times 10^9$ $M^{-1}S^{-1}$)[42,43,47]. Furthermore, the process is highly regioselective. We did not observe the formation of regioisomeric **3a'**. The observation is supported by the calculation that its formation is unfavorable by 3.8 kcal/mol due to the steric effect (Figure 5). Control experiments showed that in the absence of the HAT agent Ph_3SiSH, the yield of the dearomatized product dropped to 46% (Figure 4c). After the HAT step, the $Ph_3Si^{\bullet}$ radical is reduced by the $PC^{\bullet}$ **Mes-Acr2** radical to generate the Ph_3Si^{-} anion, which is protonated to give Ph_3SiH and the PC **Mes-Acr2** (Figure 4a).

The effect of the HAT agent is particularly noticeable in reactions of isoquinolines and naphthalenes with pyrazole. Only when PhSeH is present do these processes produce the desired products **3al** and **3ay** (Figure 4c). Furthermore, the polarity match[48] between the protic S-H/Se-H and the nucleophilic carbon radical **7a** might further facilitate the HAT process. Unexpectedly, reactions between isoquinolines and pyrazole give regioisomeric 7,8-dihydroisoquinolines. Our experiments suggest that the reaction initially forms 5,8-dihydroisoquinoline **3al'**, which is then converted to the more stable 7,8-dihydroisoquinoline **3al** (Figure 4d). The 5,8-dihydroisoquinoline **3al'** was obtained in the presence of H_2O. Two possible pathways could lead to 5,8-

dihydroisoquinoline **3al**. However, the deprotonation/C=C isomerization pathway was ruled out as we did not observe the formation of **3al** when **3al'** was treated with 2,6-lutidine, a base used in the dearomatization process. In contrast, **3al** was formed under the photoredox reaction conditions through SET oxidation of the C=C bond, deprotonation and HAT processes. This pathway was also supported by calculated reaction energies (Supplementary Figure S7).

An alternative pathway for the formation of the functionalized dearomatized product **3a** is through reduction of radical **7a** by SET from $PC^{\bullet}$ to form anion **8a**, which then undergoes protonation. However, calculations suggest that the formation of **8a** is highly unfavorable (Figure 5). Moreover, preliminary experiments showed that dearomatized product **3a** (E^{ox} = 1.60 V vs SCE, Supplementary Figure S2) could be converted back to starting material **1a** via PC^{+}* (**Mes-Acr2***) mediated oxidation under the standard reaction conditions (Figure 4c). Unexpectedly, we found that the HAT agent Ph_3SiSH retards the efficiency of this process (Figure 4c). Specifically, photoinduced reaction of **3a** in the presence of Ph_3SiSH leads to 61% recovery of **3aa** and formation of 28% of **1b**. In contrast, in the absence of the HAT agent, **1b** was produced in 49% yield. Thus, these observations indicate that the HAT agent not only facilitates the formation of dearomatized products, it also inhibits the conversion of these products back to aromatic starting materials.

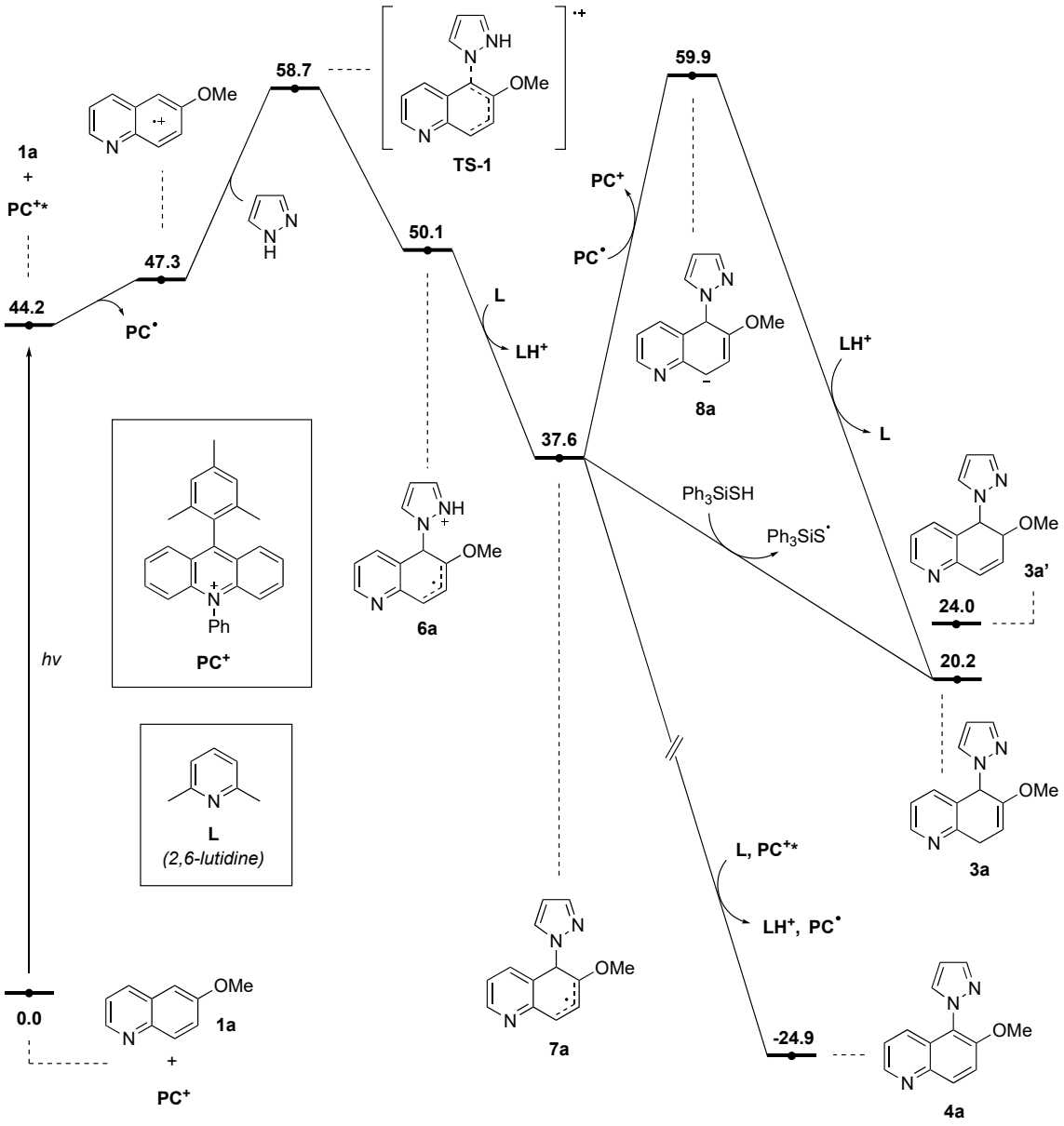

Figure 5. Calculated free energy diagram (in kcal/mol) at the ωB97X-D/def2-TZVPP, SMD (CH_2Cl_2)//ωB97X-D/def2-SVP level of theory.

In summary, we developed a conceptually unique organophotoredox catalytic dearomative functionalization strategy for the selective disruption of aromaticity in fused arenes. A reactive HAT agent is utilized to overcome the competing aromatization pathway, which is typically more favorable, and achieve the selective formation of dearomatizatized products. Experimental and computational mechanistic studies support the key role played by HAT agents in the unprecedented process. The preparative power of the protocol was demonstrated by applications to structurally

diverse fused arenes including quinolines, isoquinolines, quinoxalines, naphthalenes, anthracenes and phenanthrenes. The method can also be applied to the synthesis and late-stage skeletal editing of complex pharmaceutically valued structures. We anticipate that the new process will enable facile access to a wide range of synthetically versatile frameworks and accelerate the construction of new molecular architectures for drug discovery.

References

1. Pape, A. R., Kaliappan, K. P. & Kündig, E. P. Transition-metal-mediated dearomatization reactions. *Chem. Rev.* **100**, 2917–2940 (2000).
2. López Ortiz, F., Iglesias, M. J., Fernández, I., Andújar Sánchez, C. M. & Ruiz Gómez, G. Nucleophilic dearomatizing (DNAr) reactions of aromatic C-H systems. A mature paradigm in organic synthesis. *Chem. Rev.* **107**, 1580–1691 (2007).
3. Roche, S. P. & Porco, J. A. Dearomatization strategies in the synthesis of complex natural products. *Angew. Chem. Int. Ed.* **50**, 4068–4093 (2011).
4. Zheng, C. & You, S.-L. Advances in catalytic asymmetric dearomatization. *ACS Cen. Sci.* **7**, 432-444 (2021).
5. Huck, C. J. & Sarlah, D. Shaping molecular landscapes: recent advances, opportunities, and challenges in dearomatization. *Chem* **6**, 1589-1603 (2020).
6. Roche, S. P., Tendoung, J.-J. Y. & Tréguier, B. Advances in dearomatization strategies of indoles. *Tetrahedron* **71**, 3549-3591 (2015).
7. Zheng, C. & You, S. L. Catalytic asymmetric dearomatization (CADA) reaction-enabled total synthesis of indole-based natural products. *Nat. Prod. Rep.* **36**, 1589-1605 (2019).
8. Gentry, E. C., Rono, L. J., Hale, M. E., Matsuura, R. & Knowles, R. R. Enantioselective synthesis of pyrroloindolines via noncovalent stabilization of indole radical cations and applications to the synthesis of alkaloid natural products. *J. Am. Chem. Soc.* **140**, 3394–3402 (2018).
9. An, J., Zou, Y.-Q., Yang, Q.-Q., Wang, Q. & Xiao, W.-J. Visible light-induced aerobic oxyamidation of indoles: a photocatalytic strategy for the preparation of tetrahydro-5h-indolo[2,3-b]quinolinols. *Adv. Synth. Catal.* **355**, 1483–1489 (2013).

10. Zhu, M., Zheng, C., Zhang, X. & You, S.-L. Synthesis of cyclobutane-fused angular tetracyclic spiroindolines via visible-light-promoted intramolecular dearomatization of indole derivatives. *J. Am. Chem. Soc.* **141,** 2636–2644 (2019).
11. Ma, J., Schäfers, F., Daniliuc, C., Bergander, K., Strassert, C. A. & Frank Glorius Gadolinium photocatalysis: Dearomative [2+2] cycloaddition/ring-expansion sequence with indoles. *Angew. Chem. Int. Ed.* **59,** 9639-9645 (2020).
12. Liu, K. *et al* Electrooxidation enables highly regioselectivedearomative annulation of indole and benzofuran derivatives. *Nat. Commun.* **11**, https://doi.org/10.1038/s41467-019-13829-4 (2020).
13. Wu, J., Dou, Y., Guillot, R., Cyrille Kouklovsky, C., & Vincent, G. Electrochemical dearomative 2,3-difunctionalization of indoles. *J. Am. Chem. Soc.* **141**, 2832−2837 (2019).
14. Studies from our group and ref 15: Zhang, Y., Ji, P., Gao, F., Dong, Y., Huang, H., Wang, C., Zhou, Z., & Wang, W. Organophotocatalytic dearomatization of indoles, pyrroles and benzo(thio)furans via a Giese-type transformation. *Commun. Chem.* **4**, 20 (2021).
15. Zhang, Y., Ji, P., Gao, F., Huang, H., Zeng, F., & Wang, W. Photoredox asymmetric nucleophilic dearomatization of indoles with neutral radicals. *ACS Catal.* **11**, 998-1007 (2021)
16. Pouységu, L., Deffieux, D., & Quideau, S. Hypervalent iodine-mediated phenol dearomatization in natural product synthesis. *Tetrahedron*, **66**, 2235-2261 (2010).
17. Dhineshkumar, J., Samaddar, P., & Prabhu, K. R. A copper catalyzed azidation and peroxidation of β-naphthols via an oxidative dearomatization strategy. *Chem. Commun.* **52**, 11084-11087 (2016).
18. Kulish, K., Boldrini, C., Reis, M. C., Pérez, J. M., & Harutyunyan, S. R. Lewis acid promoted dearomatization of naphthols. *Chem. Eur. J.* **26**, 15843 (2020).
19. Sun, W., Li, G., Hong, L., & Wang, R. Asymmetric dearomatization of phenols. *Org. Biomol. Chem.* 2164-2176 (2016)
20. Zhu, G., Bao, G., Li, Y., Yang, J., Sun, W., Li, J., Hong, L., & Wang, R. Chiral phosphoric acid catalyzed asymmetric oxidative dearomatization of naphthols with quinones. *Org. Lett.* **18**, 5288-5291 (2016).
21. Takamura, M., Funabashi, K., Kanai, M., & Shibasaki, M. Asymmetric Reissert-type reaction promoted by bifunctional catalyst. *J. Am. Chem. Soc.* **122**, 6327-6328 (2000).

22. Zurro, M., Asmus, S., Beckendorf, S., Mück-Lichtenfeld, C., & Mancheño, O. G. Chiral helical oligotriazoles: new class of anion-binding catalysts for the asymmetric dearomatization of electron-deficient *N*-heteroarenes. *J. Am. Chem. Soc.* **136**, 13999-14002 (2014).
23. Pappoppula, M., Cardoso, F. S. P., Garrett, B. O., & Aponick, A. Enantioselective copper-catalyzed quinoline alkynylation. *Angew. Chem. Int. Ed.* **54,** 15202-15206 (2015).
24. Yan, X., Ge, L., Castiñeira Reis, M., & Harutyunyan, S. R. Nucleophilic dearomatization of *N*-heteroaromatics enabled by Lewis acids and copper catalysis. *J. Am. Chem. Soc.* **142**, 20247-20256 (2020).
25. Leitch, J. A., Rogova, T., Duarte, F., & Dixon, D. J. Dearomative photocatalytic construction of bridged 1,3-diazepanes. *Angew. Chem. Int. Ed.* **59**, 4121-4130 (2020).
26. Ma, J., *et al* Photochemical intermolecular dearomative cycloaddition of bicyclic azaarenes with alkenes. *Science* **371**, 1338-1345 (2021).
27. Southgate, E. H., Pospech, J., Fu, J., Holycross, D. R., & Sarlah, D. Dearomative dihydroxylation with arenophiles. *Nat. Chem.* **8,** 922-928 (2016).
28. Okumura, M., Shved, A. S., & Sarlah, D. Palladium-catalyzed dearomative *syn*-1,4-carboamination. *J. Am. Chem. Soc.* **139,** 17787-17790 (2107).
29. Hernandez, L. W., Klöckner, U., Pospech, J., Hauss, L., & Sarlah, D. Nickel-catalyzed dearomative *trans*-1,2-carboamination. *J. Am. Chem. Soc.* **140**, 4503-4507 (2018).
30. Tang, C., Okumura, M., Deng, H., & Sarlah, D. Palladium-catalyzed dearomative *syn*-1,4-oxyamination. *Angew. Chem. Int. Ed.* **58**, 15762-15766 (2019).
31. Wertjes, W. C., Okumura, M., & Sarlah, D. Palladium-catalyzed dearomative *syn*-1,4-diamination. *J. Am. Chem. Soc.* **141,** 163-167; (2019).
32. Siddiqi, Z., Wertjes, W. C. & Sarlah, D. Chemical equivalent of arene monooxygenases: dearomative synthesis of arene oxides and oxepines. *J. Am. Chem. Soc.* **142**, 10125-10131 (2020).
33. Duncton, M. A. J., Minisci reactions: Versatile CH-functionalizations for medicinal chemists. *Med. Chem. Commun.* **2**, 1135-1161 (2011).
34. Proctor, R. S. J. & Phipps, R. J. Recent advances in Minisci-type reactions. *Angew. Chem. Int. Ed.* **58**, 13666-13699 (2019).

35. Romero, N. A., Margrey, K. A., Tay, N. E., & Nicewicz, D. A. Site-selective arene C-H amination via photoredox catalysis. *Science* **349**, 1326-1330 (2015).
36. Margrey, K. A., McManus, J. B., Bonazzi, S., Zecri, F., & Nicewicz, D. A. Predictive model for site-selective aryl and heteroaryl C–H functionalization *via* organic photoredox catalysis. *J. Am. Chem. Soc.* **139,** 11288-11299 (2017).
37. McManus, J. B. & Nicewicz, D. A. Direct C–H cyanation of arenes *via* organic photoredox catalysis. *J. Am. Chem. Soc.***139,** 2880-2883 (2017).
38. Margrey, K. A., Levens, A., & Nicewicz, D. A. Direct aryl C−H amination with primary amines using organic ohotoredox catalysis. *Angew. Chem. Int. Ed.* **56**, 15644-15648 (2017).
39. Huang, H., Strater, Z. M., Rauch, M. Shee, J., Sisto, T. J., Nuckolls, C., & Lambert, T. H. Electrophotocatalysis with a trisaminocyclopropenium radical dication. *Angew. Chem. Int. Ed.* **58**, 13318-13322 (2019).
40. Zhang, L., Liardet, L., Luo, J., Ren, D., Grätzel, M., & Hu, X. Photoelectrocatalytic arene C–H amination. *Nat. Catal.* **2**, 366-373 (2019).
41. Targos, K., Williams, O. P., & Wickens, Z. K. Unveiling Potent Photooxidation Behavior of Catalytic Photoreductants. *J. Am. Chem. Soc.* **143**, 4125-4132 (2021).
42. Newcomb, M., Choi, S.-Y., & Horner, J. H. Adjusting the Top End of the Alkyl Radical Kinetic Scale. Laser Flash Photolysis Calibrations of Fast Radical Clocks and Rate Constants for Reactions of Benzeneselenol. *J. Org. Chem.* **64**, 1225-1231; (1999).
43. Newcomb, M., Varick, T. R., Ha, C., Manek, M. B., & Yue, X. Picosecond radical kinetics. Rate constants for reaction of benzeneselenol with primary alkyl radicals and calibration of the 6-cyano-5-hexenyl radical cyclization. *J. Am. Chem. Soc.* **114,** 8158-8163 (1992).
44. Xuan, J., Zhang, Z.-G., & Xiao, W.-J. Visible-light-induced decarboxylative functionalization of carboxylic acids and their derivatives. *Angew. Chem. Int. Ed.* **54**, 15632-15641 (2015).
45. Plutschack, M. B., Pieber, B., Gilmore, K., & Seeberger, P. H. The Hitchhiker's guide to flow chemistry. *Chem. Rev.* **17**, 11796-11893 (2017).
46. Rodgers, J. D., et al. Heteroaryl substituted pyrrolo[2,3-*b*]pyridines and pyrrolo[2,3-*b*]pyrimidines as Janus kinase inhibitors. **US2009181959A1**.
47. Mayer, J. M. Understanding hydrogen atom transfer: from bond strengths to Marcus theory. *Acc. Chem. Res.* **44**, 36–46 (2011).

48. Roberts, B. P. Polarity-reversal catalysis of hydrogen-atom abstraction reactions: concepts and applications in organic chemistry. *Chem. Soc. Rev.* **28**, 25–35 (1999).

Acknowledgements W.W. acknowledges the NIH (5R01GM125920) and University of Arizona for financial support and the NSF MRI for acquisition of 500 MHz NMR spectrometer (1920234). S.C. is grateful to Oberlin College for financial support. K.N.H thanks the National Science Foundation (Grant CHE-1764328). DFT calculations were performed using the SCIURus, the Oberlin College HPC cluster (NSF MRI 1427949).

Author Information P. J., F. G., J. C., and X. M. conducted and analyzed the synthetic experiments, C. C. D. performed DFT calculations under the direction of S. C., K. N. H. and W. W planned, designed and directed the project and P. J., S. C., K. N. H and W. W. wrote the manuscript.

Competing interests The authors declare no competing interests.

Additional Information Supplementary information and chemical compound information accompany this paper at www.nature.com/naturec. Reprints and permission information is available online at http://npg.nature.com/reprintsandpermission/. Correspondence and requests for materials should be addressed to K. N. H. (houk@chem.ucla.edu), S. C. (shuming.chen@oberlin.edu) and W. W. (wwang@pharmacy.arizona.edu).

Supplementary Files

This is a list of supplementary files associated with this preprint. Click to download.

- SI.pdf